Dudás *et al. BMC Medical Imaging* (2024) 24:237
https://doi.org/10.1186/s12880-024-01419-w

BMC Medical Imaging

RESEARCH

Open Access

# The reliability of virtual non-contrast reconstructions of photon-counting detector CT scans in assessing abdominal organs

Ibolyka Dudás[1], Leona Schultz[1], Márton Benke[2], Ákos Szücs[2], Pál Novák Kaposi[1], Attila Szijártó[2], Pál Maurovich-Horvat[1] and Bettina Katalin Budai[1,3*]

## Abstract

**Background** Spectral imaging of photon-counting detector CT (PCD-CT) scanners allows for generating virtual non-contrast (VNC) reconstruction. By analyzing 12 abdominal organs, we aimed to test the reliability of VNC reconstructions in preserving HU values compared to real unenhanced CT images.

**Methods** Our study included 34 patients with pancreatic cystic neoplasm (PCN). The VNC reconstructions were generated from unenhanced, arterial, portal, and venous phase PCD-CT scans using the Liver-VNC algorithm. The observed 11 abdominal organs were segmented by the TotalSegmentator algorithm, the PCNs were segmented manually. Average densities were extracted from unenhanced scans ($HU_{unenhanced}$), postcontrast ($HU_{postcontrast}$) scans, and VNC reconstructions ($HU_{VNC}$). The error was calculated as $HU_{error}=HU_{VNC}-HU_{unenhanced}$. Pearson's or Spearman's correlation was used to assess the association. Reproducibility was evaluated by intraclass correlation coefficients (ICC).

**Results** Significant differences between $HU_{unenhanced}$ and $HU_{VNC[unenhanced]}$ were found in vertebrae, paraspinal muscles, liver, and spleen. $HU_{VNC[unenhanced]}$ showed a strong correlation with $HU_{unenhanced}$ in all organs except spleen ($r=0.45$) and kidneys ($r=0.78$ and 0.73). In all postcontrast phases, the $HU_{VNC}$ had strong correlations with $HU_{unenhanced}$ in all organs except the spleen and kidneys. The $HU_{error}$ had significant correlations with $HU_{unenhanced}$ in the muscles and vertebrae; and with $HU_{postcontrast}$ in the spleen, vertebrae, and paraspinal muscles in all postcontrast phases. All organs had at least one postcontrast VNC reconstruction that showed good-to-excellent agreement with $HU_{unenhanced}$ during ICC analysis except the vertebrae (ICC: 0.17), paraspinal muscles (ICC: 0.64–0.79), spleen (ICC: 0.21–0.47), and kidneys (ICC: 0.10–0.31).

**Conclusions** VNC reconstructions are reliable in at least one postcontrast phase for most organs, but further improvement is needed before VNC can be utilized to examine the spleen, kidneys, and vertebrae.

**Keywords** Photon-counting detector, Computed tomography, Virtual non-contrast, Spectral imaging

*Correspondence:
Bettina Katalin Budai
budai.bettina.katalin@semmelweis.hu
[1]Department of Radiology, Medical Imaging Centre, Semmelweis University, 2 Korányi Sándor St, Budapest H-1083, Hungary
[2]Department of Surgery, Transplantation and Gastroenterology, Semmelweis University, 78/A Üllői St, Budapest H-1082, Hungary
[3]Department of Diagnostic and Interventional Radiology, Heidelberg University Hospital, Im Neuenheimer Feld 130.3, 69120 Heidelberg, Germany

## Background

The technology of photon counting by single photon detectors has been around for decades in quantum information science. However, in the field of human medicine, the first photon-counting detector CT scanner (PCD-CT) has only recently been introduced. This detector system enables acquiring spectral information from the imaged structures that makes the subtraction of iodine from the postcontrast scans possible generating virtual non-contrast (VNC) reconstructions during post-processing [1]. A more detailed description of this technology can be found in the article by Flohr et al. [2].

The introduction of PCD-CT scanners in clinical practice paved the way for clinical research [3]. In abdominal imaging, the assessment of certain findings such as hepatic steatosis [4], chronic calcifying pancreatitis [5], and kidney stones [6] requires unenhanced CT scans before contrast material administration. A common assumption is that reliable VNC reconstructions generated from the postcontrast CT scans could be used in the future to replace real unenhanced phase CT scans reducing the radiation dose of patients.

The reliability of VNC reconstructions of dual-energy CT scanners is a widely researched area [7–9], however, only a handful of studies investigated the applicability and reliability of VNC maps of the novel PCD-CT in abdominal imaging involving the analysis of multiple organs [10–12]. By the subjective 5-point scale analysis of the image quality, subjective image noise, and noise texture, Mergen et al. reported that VNC reconstructions may have a lower image quality compared to real unenhanced abdominal scans, however with only a moderate interobserver agreement [10]. Previous publications that have quantitatively validated the reliability of VNC reconstructions of PCD-CT scanners have mainly focused on comparing the average Hounsfield units (HU) density values of the investigated organs. Niehoff et al. [11] assessed selected regions of interest (ROIs) of the liver, spleen, kidney, vertebrae, paraspinal muscles, aorta, and fat and reported significant differences between VNC reconstructions vs. real unenhanced scans in both the arterial and venous phase scans for all the investigated organs. In a similar study, Schoenbeck et al. [12] investigated selected ROIs of the liver, spleen, renal cortex, aorta, paraspinal muscles, and subcutaneous fat and they compared the performance of the prior VNC algorithm and the later Liver-VNC algorithm. The authors found significant differences between the real unenhanced scans and their VNC reconstructions in the liver, renal cortex, aorta, paraspinal muscle, and subcutaneous fat, but reported no significant differences in the spleen using the VNC algorithm. Moreover, when comparing the VNC reconstructions of the portal venous phase scans to the real unenhanced ones, the authors found significant differences in all organs except the paraspinal muscles whether the earlier VNC or the later Liver-VNC algorithm was used. However, these previous studies accessed only manually selected circular ROIs of the investigated organs, cystic structures were not evaluated, and it was not assessed whether the error of the reconstruction algorithm shows correlations with the baseline density and the contrast-enhancement of the organs.

In our study, we have enrolled patients diagnosed with pancreatic cystic neoplasm (PCN) as this patient population requires regular follow-up imaging and therefore could benefit significantly from radiation dose reduction if unenhanced phase scans could be replaced with VNC reconstructions in the future. To the best of our knowledge, the reliability of VNC reconstructions of PCD-CT scanners has not yet been investigated in this special population. Investigating PCNs besides other abdominal organs also allows for the reliability assessment of the algorithm in the case of cystic structures and small calcifications. Therefore our study had a special focus on the evaluation of VNC reconstructions' image quality affecting the radiological assessment of these small calcifications.

We aimed to investigate the reliability of VNC of triple-phasic scans compared to real unenhanced scans. Our study covers the semiquantitative and quantitative evaluation of 12 abdominal organs. We also aimed to investigate the correlation of the density error with the baseline density and the contrast enhancement of organs. Finally, we also aimed to illustrate the most common pitfalls of the reconstruction algorithm, which should be kept in mind when using it.

## Methods

### Patient population

Our study was approved by the institutional ethics committee. The study adheres to the World Medical Association guidelines and the Declaration of Helsinki, revised in 2000 in Edinburgh. As this is a retrospective study, the need for written informed patient consent was waived by the ethics committee. All patient data were analyzed anonymously.

Follow-up PCD-CT scans from consecutive PCN patients were retrospectively collected between March 2022 – May 2023. Consecutive patients in this time frame were retrospectively identified, who were diagnosed and followed for PCN in the Surgery Department of our University in accordance with the European evidence-based Guidelines of the European Study Group on Cystic Tumours of the Pancreas [13] and who were referred for follow-up CT examination to our Medical Imaging Centre after the installation of the new PCD-CT scanner. CT scans of these patients that were carried out in the considered time frame due to indications other than the regular follow-up were not included. 73 patients were scanned during their follow-up, which led to 86 CTs, whereas 11 patients had two and 1 patient had 3 CT examinations. One scan was excluded due to the incomplete coverage of the PCN. A further six cases were excluded because the PCN could not be contoured due to undefined, blurred tumor margins. The unenhanced phase scans of 44 scans could not be reconstructed with spectral information due to technical issues that resulted in data loss. Therefore, the final patient cohort consisted of 34 patients with 35 CTs. Figure 1 demonstrates the patient selection and data analysis strategy.

## Imaging protocol

The patients were examined at our Institution with a PCD-CT scanner (NAEOTOM Alpha, VA50; Siemens Healthineers) according to our routine pancreas imaging protocol that included an unenhanced scan, followed by an arterial phase, a portal venous phase, and a venous phase postcontrast scan. The scans were performed with a tube voltage of 120 kVp and an automated tube current modulation. The rotation time was 0.5 s, the pitch was 0.80, the single collimation width was 0.40 mm, the total collimation width was 144×0.40 mm, and the reconstruction matrix was 512×512 for all scans.

For the contrast-enhanced scans, an iodinated non-ionic contrast agent (either Ultravist 370 or Iomeron 350) was applied using a power injector followed by a 40 mL saline chaser. A power injector that automatically adjusts the injection flow rates by monitoring the peak pressures was used, therefore, the actual contrast injection flow rate was dependent on patient-specific factors such as cardiovascular state, hydration status, etc. resulting in injection flow rates of 2.7–4.4 mL/s in the patient cohort. The amount of contrast agent was adjusted to the patient's body weight. The amount of iodine injected was 340±52 mg iodine/kg in the patient cohort. Automated timing of the contrast injection was performed with a bolus tracking technique triggered by the peak contrast enhancement measured in the thoracic aorta with a manually placed circular ROI. The timing for the arterial, portal, and venous phase scans were 23 s, 45 s, and 75 s, respectively.

The arterial phase scans were acquired from above the diaphragm to the iliac crest, the portal phase scans were focused on the pancreas covering the upper abdomen, while the unenhanced and the venous phase postcontrast scans were acquired from above the diaphragm to below the symphysis. The field-of-view was manually set by the radiographer to cover the entire body on the axial view.

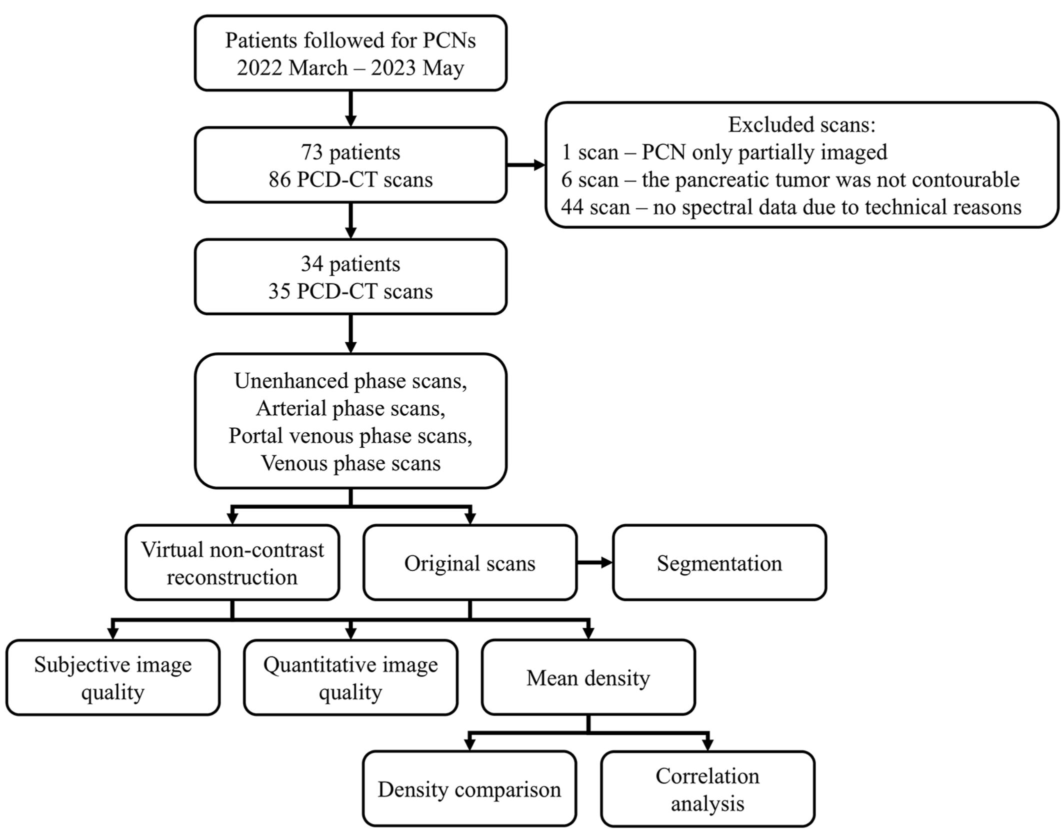


**Fig. 1** Flowchart on the main steps of the study. PCD-CT: photon-counting detector CT; PCN: pancreatic cystic neoplasm

The CT scans were reconstructed in the axial plane with the so-called spectral post-processing (SPP) reconstruction algorithm of the vendor that preserves all the spectral information. A Qr40 soft kernel with a quantum iterative reconstruction algorithm at a strength level of 3 was used. All scans were reconstructed with a slice thickness of 2.0 mm and an increment of 1.5 mm.

### Image postprocessing and segmentation

The VNC images were reconstructed with the Liver-VNC algorithm of the dedicated eXamine research software (Siemens Healthineers, Forchheim, Germany) using the manufacturer's default settings: the thresholds on high energy bin (65 keV) reconstruction were −92 HU for fat and 58 HU for soft tissues, these values on low energy bin (20 keV) reconstruction were −100 HU for fat and 59 HU for soft tissue, while the applied iodine enhancement ratio was 2.0. We used the Liver-VNC algorithm instead of the previous VNC algorithm of the manufacturer. While the previous VNC algorithm performs material decomposition based on the separation of air, iodine, and water; the Liver-VNC algorithm has been developed to take into account fat and soft tissue in addition to the iodine contrast agent to provide a more appropriate algorithm for abdominal organs.

Further processing was completed using the 3D Slicer software v5.2.2 [14]. The covered body regions on the unenhanced, arterial phase, portal phase, and venous phase postcontrast scans showed differences, theredore, for direct comparison, all scans were manually cropped to get the same volumes covering the upper abdomen (Supplementary Fig. 1 of Additional file 1). The three-dimensional volume of the pancreas parenchyma, liver, spleen, iliopsoas muscles, erector spinae muscles, L1 and L2 vertebra, and kidneys were segmented in an artificial intelligence-assisted manner using the TotalSegmentator algorithm [15]. Manual corrections were made to the segmentation masks where necessary. Manual slice-by-slice segmentation of the PCNs was performed by an expert radiologist with over 10 years of experience (Supplementary Fig. 1 of Additional file 1), the area of the PCN was then subtracted from the area of the pancreas parenchyma segmented by the TotalSegmentator algorithm to avoid overlap. In all cases, the segmentation was performed on the original scans, and the same segmentation masks were applied to the corresponding VNC reconstructions since the Liver-VNC algorithm does not change the spatial location of the corresponding voxels. In order to assess the signal-to-noise ratio (SNR) and contrast-to-noise ratio (CNR) of the real unenhanced scans as well as the VNC reconstructions, 3 circular ROIs were manually placed to the subcutaneous fat at the middle level of the L3 vertebra on all scans in approximately the same position (Supplementary Fig. 2 of Additional file 1). The size of the ROIs was kept to the maximum, however, it was dependent on the thickness of the subcutaneous fat, therefore the diameter of the circular ROIs was between 9.6 and 31.0 mm.

### Quantitative image analysis

During quantitative image analysis, the 70 keV virtual monoenergetic reconstructions of the real unenhanced CT scans were used as reference standards. In this study, the SPP reconstructions of the unenhanced scans that contain all the spectral information were investigated instead of the polyenergetic T3D reconstructions to demonstrate the pure effect of the Liver-VNC algorithm avoiding the influence of the different reconstruction algorithms (SPP vs. T3D) on the results. The reliability of the VNC reconstructions was evaluated by assessing the mean HU density values extracted from the entire volume of the organs. The VNC reconstructions of the real unenhanced scans were also generated to assess the extent to which the algorithm changes the density of organs during iodine subtractions from scans that contain no iodine contrast. The error of the Liver-VNC algorithm ($HU_{error}$) was calculated as the difference between the mean density on the VNC reconstruction ($HU_{VNC}$) and the mean density on the corresponding real unenhanced phase scan ($HU_{unenhanced}$) as proposed by Holz et al. [16].

$$HU_{error} = HU_{VNC} - HU_{unenhanced}$$

By manually placing 3 circular ROIs in the subcutaneous tissue at the middle level of the L3 vertebra (Supplementary Fig. 2), the mean and the standard deviation (SD) of the HU values were extracted, and the average of the 3 measurements was calculated.

The SNR was defined as the ratio of the mean density and the SD of the voxels of the given organ. The CNR was defined as the difference between the mean density of the given organ and the mean density of the subcutaneous fat, divided by the SD of the voxels of the subcutaneous fat similar to those formulas previously published by Al-Difaie et al. [17] and Si-Mohamed et al. [18].

$$SNR = mean_{tissue}/SD_{tissue}$$

$$CNR = \frac{mean_{tissue} - mean_{fat}}{SD_{fat}}$$

The calculated SNR and CNR values of the arterial phase VNC ($SNR_{VNC[arterial]}$, $CNR_{VNC[arterial]}$), portal venous phase VNC ($SNR_{VNC[portal]}$, $CNR_{VNC[portal]}$), venous phase VNC ($SNR_{VNC[venous]}$, $CNR_{VNC[venous]}$), as well as the unenhanced phase VNC ($SNR_{VNC[unenhanced]}$, $CNR_{VNC[unenhanced]}$) were directly compared to the

SNR and CNR values of the real unenhanced scans ($SNR_{unenhanced}$, $CNR_{unenhanced}$).

For easier interpretability, we summarized the introduced terms of measured HU density values and calculated ratios in Table 1.

The main steps of the data analysis are summarized in Fig. 1. The extracted density values of the organs can be found in Additional file 2.

### Subjective reading of CT reconstructions

An expert radiologist with over 10 years of experience performed the side-by-side subjective reading of the unenhanced phase CT scans and the VNC reconstructions. The radiologist was asked to review the presence of pancreatic calcifications, central/mural calcifications of PCNs, and kidney stones, and measure their largest diameter on the real unenhanced scans and VNC reconstructions using the standard bone window. The image quality was then subjectively evaluated by the radiologist based on a 5-point scale; where the 5-point maximum means that the image quality in evaluating the calcification is equal with the real unenhanced phase scan; 4-point means that the image quality is worse but it does not affect the radiological evaluation; 3-point means that the image quality is markedly worse which may affect the radiological evaluation; 2-point means the calcification is barely visible which severely violates the radiological evaluation; and 1-point means the calcification is fully subtracted, not visible. The number of calcified lesions did not allow for detailed statistical evaluation, however, we demonstrate the limitations of the VNC reconstructions in these cases.

**Table 1** Abbreviations used for Hounsfield unit density measurements of different scans and reconstructions

| Abbreviation | Meaning |
| --- | --- |
| $HU_{VNC}$ | Average density measured on the virtual non-contrast reconstruction. |
| $HU_{VNC[unenhanced]}$ | Average density measured on the virtual non-contrast reconstruction generated from the unenhanced phase scans. |
| $HU_{VNC[arterial]}$ | Average density measured on the virtual non-contrast reconstruction generated from the arterial phase scans. |
| $HU_{VNC[portal]}$ | Average density measured on the virtual non-contrast reconstruction generated from the portal venous phase scans. |
| $HU_{VNC[venous]}$ | Average density measured on the virtual non-contrast reconstruction generated from the venous phase scans. |
| $HU_{unenhanced}$ | Average density measured on the real unenhanced phase scans. |
| $HU_{postcontrast}$ | Average density measured on the postcontrast scans. |
| $HU_{arterial}$ | Average density measured on the arterial phase postcontrast scans. |
| $HU_{portal}$ | Average density measured on the portal venous phase postcontrast scans. |
| $HU_{venous}$ | Average density measured on the venous phase postcontrast scans. |
| $HU_{error}$ | The difference between $HU_{VNC}$ and $HU_{unenhanced}$. |
| $HU_{error[unenhanced]}$ | The difference between $HU_{VNC[unenhanced]}$ and $HU_{unenhanced}$. |
| $HU_{error[arterial]}$ | The difference between $HU_{VNC[arterial]}$ and $HU_{unenhanced}$. |
| $HU_{error[portal]}$ | The difference between $HU_{VNC[portal]}$ and $HU_{unenhanced}$. |
| $HU_{error[venous]}$ | The difference between $HU_{VNC[venous]}$ and $HU_{unenhanced}$. |

### Statistical analysis

The density values of the CT scans and VNC reconstructions are reported in HU. During statistical analysis, the Shapiro-Wilk test was used to test normality, followed by Levene's test for the assessment of the homogeneity of variances between groups. For the comparison of paired groups, either the paired sample t-test or the Wilcoxon signed-rank test was used to compare the mean density values. Correction for multiple testing was applied according to the Benjamini-Hochberg method. A threshold of $p<0.05$ was used to decide the statistical significance of all comparisons. The values are reported as mean ± standard deviation. Pearson's correlation coefficient (r) or Spearman's rho was used to assess the correlation of $HU_{error}$ with the contrast enhancement of organs on the postcontrast scans ($HU_{postcontrast}$) and the $HU_{unenhanced}$. The correlations were classified as weak ($r$=0.20–0.39), moderate ($r$=0.40–0.59), strong ($r$=0.60–0.79), and very strong ($r$=0.80-1.00). The reproducibility of the measurements was evaluated based on the mean and 95% confidence interval (CI) values of the intraclass correlation coefficient (ICC) by using a 2-way random effect, single-measurement, absolute-agreement model (ICC 2,1). Bland-Altman plots were used for visualizing the differences between $HU_{VNC}$ and $HU_{unenhanced}$.

The statistical analysis was completed with dedicated packages coded in Python such as "numpy", "pandas", "sklearn", "scipy", "statsmodels", "seaborn", and "matplotlib".

## Results

### Patient population

The final patient cohort included 34 patients, of whom 19 were diagnosed with intraductal papillary mucinous neoplasms, 4 with mucinous cystic neoplasms, 4 with serous cystic neoplasms, 3 with adenocarcinomas, 1 with solid pseudopapillary neoplasm, 1 with cystic pancreatic neuroendocrine tumor, 1 with lymphoepithelial tumor, and 1 with unclassified PCN without worrisome features. One patient with serous cystic neoplasm had 2 follow-up CT scans.

The contrast material routinely used in our CT laboratory was changed during the investigated period due to institutional factors; therefore, during contrast-enhanced CT examination, the Ultravist 370 contrast agent was used for 16 patients, while 19 patients received the Iomeron 350 contrast material. Table 2. summarizes the demographic data of the patient cohort.

#### Comparison of the mean density values

The violin plots on the differences between the mean densities on the arterial phase ($HU_{VNC[arterial]}$), portal phase ($HU_{VNC[portal]}$), and venous phase ($HU_{VNC[venous]}$) VNC reconstructions vs. densities on the real unenhanced scans ($HU_{unenhanced}$) can be found in Additional file 1 (Supplementary Figs. 3–6). The correlation plots on the association between $HU_{VNC}$ and $HU_{unenhanced}$ as well as the Bland-Altman plots illustrating the association of $HU_{error}$ with the organs' average HU density can be found in Additional file 1 (Supplementary Figs. 7–18 and Supplementary Figs. 19–22). All organs had at least one contrast phase that reached a strong correlation except the spleen and kidneys. Moreover, the correlation for the spleen in the portal venous phase did not reach statistical significance.

**Table 2** Descriptive data of the patient cohort

| | All | Male | Female |
|---|---|---|---|
| n | 34 | 12 (35.3%) | 22 (64.7%) |
| Age (years) | 64.4 ± 15.0 | 71.0 ± 15.5 | 60.9 ± 13.9 |
| Weight (kg) | 77.6 ± 15.2 | 86.2 ± 12.7 | 72.2 ± 14.3 |
| Hight (cm) | 169.3 ± 9.8 | 176.1 ± 9.6 | 164.6 ± 7.0 |
| BMI (kg/m$^2$) | 27.1 ± 4.5 | 28.0 ± 3.9 | 26.5 ± 4.9 |
| eGFR | 73.7 ± 18.9 | 68.8 ± 22.0 | 77.0 ± 16.5 |
| Effective tube current - unenhanced (mAs) | 121.1 ± 41.6 | 131.2 ± 22.7 | 115.1 ± 49.2 |
| Effective tube current - arterial (mAs) | 134.1 ± 48.2 | 151.8 ± 26.9 | 123.5 ± 55.3 |
| Effective tube current - portal (mAs) | 94.3 ± 36.5 | 107.3 ± 21.2 | 86.6 ± 41.8 |
| Effective tube current - venous (mAs) | 100.4 ± 29.7 | 102.3 ± 16.4 | 99.3 ± 35.8 |
| $CTDI_{vol}$- unenhanced (mGy) | 12.7 ± 18.6 | 10.3 ± 1.8 | 13.9 ± 23.0 |
| $CTDI_{vol}$- arterial (mGy) | 10.7 ± 3.6 | 11.9 ± 2.1 | 10.1 ± 4.1 |
| $CTDI_{vol}$- portal (mGy) | 7.5 ± 2.7 | 8.4 ± 1.7 | 7.0 ± 3.1 |
| $CTDI_{vol}$- venous (mGy) | 8.0 ± 2.3 | 8.0 ± 1.3 | 8.0 ± 2.7 |
| DLP - unenhanced (mGy · cm) | 357.3 ± 200.3 | 403.8 ± 120.5 | 329.5 ± 234.3 |
| DLP - arterial (mGy · cm) | 297.8 ± 124.8 | 352.9 ± 90.8 | 264.7 ± 132.5 |
| DLP - portal (mGy · cm) | 176.3 ± 70.4 | 215.0 ± 63.8 | 153.1 ± 64.9 |
| DLP - venous (mGy · cm) | 383.9 ± 125.4 | 403.8 ± 73.50 | 372.0 ± 148.7 |

The results are reported as mean ± standard deviation

BMI: body mass index; CTDI: DT dose index; DLP: dose length product; eGFR: estimated glomerular filtration rate

#### Comparison of real unenhanced with unenhanced VNC reconstructions

The $HU_{VNC[unenhanced]}$ of the spleen, liver, and paraspinal muscles were significantly ($p < 0.0001$) higher, while those of the vertebrae were significantly lower ($p < 0.0001$) compared to the $HU_{unenhanced}$ values (Table 3). However, the $HU_{error}$ for the spleen and liver were only 2.35 ± 2.70 and 4.97 ± 2.94 HU, respectively. The $HU_{VNC[unenhanced]}$ values showed very strong correlations with the $HU_{unenhanced}$ values in all organs except the kidneys ($r = 0.78$ and 0.73; $p < 0.0001$) and the spleen ($r = 0.45$; $p = 0.0065$) (Table 4).

#### Analysis of the vertebrae

In all postcontrast VNC reconstructions, the most marked $HU_{error}$ was found in the vertebrae, where the algorithm struggled to differentiate calcium from iodine which resulted in significantly ($p < 0.0001$) lower density values on the VNC reconstructions (Table 3). The $HU_{VNC}$ values had very strong correlations with the $HU_{unenhanced}$ (Table 4). The $HU_{error}$ also showed very strong correlations with the $HU_{postcontrast}$ and $HU_{unenhanced}$ (Table 5).

#### Analysis of the kidneys

There was no significant difference between $HU_{unenhanced}$ and $HU_{VNC[unenhanced]}$ in the kidneys. However, the difference between $HU_{unenhanced}$ and $HU_{VNC}$ was significant ($p < 0.0001$) for both kidneys in all postcontrast phases (Table 3) with a $HU_{error}$ of -4.80 ± 4.05HU for the left and −4.53 ± 4.75HU for the right kidneys in the arterial phase. The $HU_{error}$ was markedly higher in the portal phase and even higher in the venous phase (Table 3). Moreover, the $HU_{VNC}$ values had only a moderate correlation with the $HU_{unenhanced}$ values (Table 4), and the $HU_{error}$ also had a moderate association with the $HU_{arterial}$ and a weak to moderate correlation with the $HU_{venous}$ (Table 5).

In the arterial phase, 19/35 and 18/35 cases had a $HU_{error}$ less than ±5 HU, and an additional 12/35 and 13/35 had a maximum $HU_{error}$ of ±10 HU. In the portal venous phase, these were 9/35, 10/35, and 8/35, 6/35, respectively. While in the venous phase, 5/35 and 9/35 cases were within the range of ±5 HU, and an additional 11/35 and 6/35 had a maximum $HU_{error}$ of ±10 HU. The histograms illustrating the number of patients in each category can be found in Additional file 1 (Supplementary Fig. 23).

#### Analysis of the paraspinal and iliopsoas muscles

The $HU_{error}$ dominantly resulted in positive values for the paraspinal muscles and the difference between $HU_{unenhanced}$ and $HU_{VNC}$ was significant in all phases. Meanwhile, the $HU_{error}$ of the iliopsoas muscles consistently resulted in negative values but the difference reached significance in only the portal and venous phases (Table 3). The $HU_{VNC}$ values had very strong correlations

**Table 3** Density differences between VNC reconstructions vs. real unenhanced phase scans, and the correlation with the enhancement on postcontrast phase scans

| | Unenhanced | Unenhanced phase VNC | | | Arterial phase VNC | | | Portal phase VNC | | | Venous phase VNC | | |
|---|---|---|---|---|---|---|---|---|---|---|---|---|---|
| **Organ** | **Mean (HU)** | **Mean (HU)** | **$HU_{error}$ (HU)** | ***p*-value*** | **Mean (HU)** | **$HU_{error}$ (HU)** | ***p*-value*** | **Mean (HU)** | **$HU_{error}$ (HU)** | ***p*-value*** | **Mean (HU)** | **$HU_{error}$ (HU)** | ***p*-value*** |
| **Spleen** | 44.95 ± 2.26 | 47.30 ± 2.82 | 2.35 ± 2.70 | **< 0.0001** | 46.59 ± 3.24 | 1.64 ± 2.66 | **0.001** | 42.37 ± 4.74 | -2.58 ± 4.54 | **0.002** | 45.26 ± 2.96 | 0.31 ± 2.74 | 0.840 |
| **Right kidney** | 28.48 ± 3.17 | 28.23 ± 4.77 | -0.25 ± 3.06 | 0.790 | 23.68 ± 4.90 | -4.80 ± 4.05 | **< 0.0001** | 19.02 ± 7.51 | -9.46 ± 6.52 | **< 0.0001** | 16.67 ± 7.16 | -11.81 ± 6.42 | **< 0.0001** |
| **Left kidney** | 27.2 ± 3.1 | 27.01 ± 4.35 | -0.22 ± 2.98 | 0.726 | 22.7 ± 5.4 | -4.53 ± 4.75 | **< 0.0001** | 18.4 ± 8.5 | -8.86 ± 7.31 | **< 0.0001** | 16.2 ± 8.0 | -11.01 ± 6.97 | **< 0.0001** |
| **Liver** | 52.69 ± 8.75 | 57.66 ± 9.62 | 4.97 ± 2.94 | **< 0.0001** | 57.33 ± 9.33 | 4.64 ± 2.85 | **< 0.0001** | 54.81 ± 8.64 | 2.12 ± 2.60 | **< 0.0001** | 55.19 ± 8.61 | 2.50 ± 2.22 | **< 0.0001** |
| **Pancreas** | 23.83 ± 11.33 | 24.72 ± 11.00 | 0.89 ± 4.29 | 0.304 | 22.36 ± 10.76 | -1.47 ± 4.87 | 0.083 | 18.90 ± 11.24 | -4.9 ± 5.9 | **< 0.0001** | 20.50 ± 10.72 | -3.33 ± 2.95 | **< 0.0001** |
| **L2 vertebra** | 339.19 ± 82.80 | 160.45 ± 41.76 | -178.75 ± 46.18 | **< 0.0001** | 163.65 ± 43.20 | -175.54 ± 46.22 | **< 0.0001** | 164.84 ± 44.58 | -174.36 ± 45.36 | **< 0.0001** | 161.82 ± 43.67 | -177.37 ± 45.90 | **< 0.0001** |
| **L1 vertebra** | 324.26 ± 76.58 | 156.69 ± 38.99 | -167.57 ± 42.57 | **< 0.0001** | 159.87 ± 40.53 | -164.39 ± 42.25 | **< 0.0001** | 161.38 ± 41.95 | -162.88 ± 41.50 | **< 0.0001** | 158.61 ± 41.36 | -165.65 ± 41.69 | **< 0.0001** |
| **Left erector spinae** | 32.06 ± 12.12 | 37.62 ± 11.62 | 5.57 ± 2.90 | **< 0.0001** | 38.46 ± 11.14 | 6.40 ± 2.93 | **< 0.0001** | 37.24 ± 11.27 | 5.18 ± 2.87 | **< 0.0001** | 36.89 ± 11.25 | 4.83 ± 2.70 | **< 0.0001** |
| **Right erector spinae** | 32.39 ± 11.40 | 37.85 ± 10.86 | 5.46 ± 2.85 | **< 0.0001** | 38.58 ± 10.66 | 6.18 ± 2.76 | **< 0.0001** | 37.15 ± 10.73 | 4.76 ± 2.70 | **< 0.0001** | 36.84 ± 10.67 | 4.45 ± 2.57 | **< 0.0001** |
| **Left iliopsoas** | 45.68 ± 5.34 | 44.48 ± 5.28 | -1.19 ± 3.28 | 0.067 | 44.29 ± 5.19 | -1.38 ± 3.25 | **0.020** | 43.06 ± 4.96 | -2.61 ± 2.76 | **< 0.0001** | 42.55 ± 4.89 | -3.12 ± 2.8033 | **< 0.0001** |
| **Right iliopsoas** | 44.10 ± 5.23 | 43.07 ± 5.32 | -1.03 ± 3.18 | 0.094 | 43.01 ± 4.75 | -1.09 ± 3.44 | 0.076 | 41.60 ± 4.62 | -2.51 ± 3.16 | **< 0.0001** | 40.78 ± 4.57 | -3.32 ± 3.21 | **< 0.0001** |
| **PCN** | 14.34 ± 8.34 | 14.77 ± 9.31 | 0.43 ± 3.87 | 0.623 | 10.53 ± 10.45 | -3.81 ± 5.76 | **0.001** | 6.11 ± 10.43 | -8.24 ± 7.72 | **< 0.0001** | 7.12 ± 9.76 | -7.22 ± 6.09 | **< 0.0001** |

* p-value corrected according to the Benjamini-Hochberg method

The results are reported as mean±standard deviation

HU: Hounsfield Unit; PCN: pancreatic cystic neoplasm; VNC: virtual non-contrast reconstruction

**Table 4** Correlation between the density values of real unenhanced scans and VNC reconstructions

| | $HU_{VNC[unenhanced]}$ | | $HU_{VNC[arterial]}$ | | $HU_{VNC[portal]}$ | | $HU_{VNC[venous]}$ | |
|---|---|---|---|---|---|---|---|---|
| **Organ** | | ***p*-value** | ***r*** | ***p*-value** | ***r*** | ***p*-value** | ***r*** | ***p*-value** |
| **Spleen** | 0.45 | **0.0065** | 0.5826 | **0.0002** | 0.3279 | 0.0545 | 0.4381 | **0.0085** |
| **Right kidney** | 0.78 | **< 0.0001** | 0.5688 | **0.0004** | 0.5018 | **0.0021** | 0.4431 | **0.0077** |
| **Left kidney** | 0.73 | **< 0.0001** | 0.4768 | **0.0038** | 0.5377 | **0.0009** | 0.5089 | **0.0018** |
| **Liver** | 0.92 | **< 0.0001** | 0.9308 | **< 0.0001** | 0.9331 | **< 0.0001** | 0.9398 | **< 0.0001** |
| **Pancreas** | 0.93 | **< 0.0001** | 0.9039 | **< 0.0001** | 0.8943 | **< 0.0001** | 0.9658 | **< 0.0001** |
| **L2 vertebra** | 0.94 | **< 0.0001** | 0.9347 | **< 0.0001** | 0.9300 | **< 0.0001** | 0.9311 | **< 0.0001** |
| **L1 vertebra** | 0.93 | **< 0.0001** | 0.9210 | **< 0.0001** | 0.9235 | **< 0.0001** | 0.9258 | **< 0.0001** |
| **Left erector spinae** | 0.97 | **< 0.0001** | 0.9719 | **< 0.0001** | 0.9726 | **< 0.0001** | 0.9761 | **< 0.0001** |
| **Right erector spinae** | 0.97 | **< 0.0001** | 0.9710 | **< 0.0001** | 0.9720 | **< 0.0001** | 0.9749 | **< 0.0001** |
| **Left iliopsoas** | 0.81 | **< 0.0001** | 0.8098 | **< 0.0001** | 0.8595 | **< 0.0001** | 0.8536 | **< 0.0001** |
| **Right iliopsoas** | 0.82 | **< 0.0001** | 0.7663 | **< 0.0001** | 0.8002 | **< 0.0001** | 0.7939 | **< 0.0001** |
| **PCN** | 0.91 | **< 0.0001** | 0.8354 | **< 0.0001** | 0.6827 | **< 0.0001** | 0.7847 | **< 0.0001** |

HU: Hounsfield Unit; PCN: pancreatic cystic neoplasm; VNC: virtual non-contrast reconstruction

with the $HU_{unenhanced}$ values in both phases for the paraspinal muscles, while the iliopsoas muscles showed strong to very strong correlations (Table 4). The $HU_{error}$ in the paraspinal muscles showed weak to moderate correlations with the $HU_{arterial}$, $HU_{portal}$, and $HU_{venous}$ values, while in the iliopsoas muscles, a significant correlation was only found in the venous phase (Table 5). In both three phases, the $HU_{error}$ had weak but significant correlations with $HU_{unenhanced}$ values for all muscles except the left iliopsoas in the venous phase and right iliopsoas in the portal phase (Table 5).

The $HU_{error}$ was within the range of a maximum of ±15 HU values in all phases for all muscles. For the paraspinal muscles, 10/35 cases were within the range of ±5 HU in the arterial phase, 15/35 were within this range in the portal venous phase, while in the venous phase, it was 17/35 cases. The iliopsoas muscles showed better results, 30/35 and 29/35 cases were within the range of ±5 HU in the arterial phase, 29/35 were within this range in the portal venous phase, while in the venous phase, it was 28/35 and 26/35 cases for the right and left muscles, respectively. The histograms illustrating the number of patients in each category can be found in Additional file 1 (Supplementary Fig. 23).

### Analysis of the pancreas and PCNs

The analysis of the pancreas revealed no significant differences between $HU_{unenhanced}$ and $HU_{VNC[arterial]}$ (Table 3). The $HU_{VNC}$ values showed very strong correlations with the $HU_{unenhanced}$ values in all phases (Table 4). Moreover, no correlation was found between $HU_{error}$ and either $HU_{unenhanced}$, $HU_{arterial}$, $HU_{portal}$, or $HU_{venous}$ (Table 5).

In the arterial phase, the $HU_{error}$ values were within the range of ±5 HU in 29/53 cases, while all but one cases were within the range of ±10 HU. In the portal venous phase, 20/35 cases had a maximum $HU_{error}$ of ±5 HU, while an additional 12/35 were within the range of ±10 HU. Similar results were found in the venous phase with 26/35 cases within the range of ±5 HU and an additional 8/35 cases within the range of ±10 HU. The PCNs showed the best results on the arterial phase, where the $HU_{error}$ was within the range of ±5 HU in 18/35 cases, and an additional 11/35 had a maximum $HU_{error}$ of ±10 HU. The worst $HU_{error}$ results were observed in the portal phase, where 7/35 cases were out of the range of ±15 HU. The histograms illustrating the number of patients in each category can be found in Additional file 1 (Supplementary Fig. 23).

The analysis of the PCNs revealed significant differences between $HU_{unenhanced}$ and both $HU_{VNC[arterial]}$, $HU_{VNC[portal]}$, and $HU_{VNC[venous]}$, however, the difference in the arterial phase was only −3.81±5.76 HU (Table 3). The $HU_{VNC[arterial]}$ had a very strong, while the $HU_{VNC[venous]}$ and the $HU_{portal-VNC}$ had strong correlations with the $HU_{unenhanced}$ (Table 4). The $HU_{error}$ showed a significant correlation only with the $HU_{arterial}$ values, no correlation was found with $HU_{unenhanced}$ in either phase (Table 5).

### Analysis of the spleen

In the spleen, significant differences were detected between $HU_{unenhanced}$ and $HU_{VNC}$ in all phases, although the $HU_{error}$ was only 1.64±2.66 HU in the arterial phase (Table 3). The $HU_{VNC}$ had only a moderate correlation with the $HU_{unenhanced}$ on the arterial and venous phases, while no correlation was found in the portal phase (Table 4). Moreover, the $HU_{error}$ also had significant, strong correlations with $HU_{arterial}$ and $HU_{portal}$, and a moderate correlation with $HU_{venous}$ (Table 5).

In the arterial phase, 23/35 cases had a $HU_{error}$ less than ±5 HU, and all the cases were within the range of ±10 HU. In the portal venous phase, 23/35 were within the range of ±5 HU, an additional 9/35 had a maximum $HU_{error}$ of ±10 HU, while the remaining 3/35 had a

**Table 5** Correlation of the density differences between real unenhanced scans and VNC reconstructions ($HU_{error}$) vs (1) densities on the real unenhanced phase scans, and (2) the enhancement on postcontrast phase scans

| | Arterial phase $HU_{error}$ | | | | Portal phase $HU_{error}$ | | | | Venous phase $HU_{error}$ | | | |
|---|---|---|---|---|---|---|---|---|---|---|---|---|
| | $HU_{unenhanced}$ | | $HU_{arterial}$ | | $HU_{unenhanced}$ | | $HU_{portal}$ | | $HU_{unenhanced}$ | | $HU_{venous}$ | |
| **Organ** | ***r*** | ***p*-value** | ***r*** | ***p*-value** | ***r*** | ***p*-value** | ***r*** | ***p*-value** | ***r*** | ***p*-value** | ***r*** | ***p*-value** |
| **Spleen** | -0.1399 | 0.4229 | -0.7248 | **< 0.0001** | -0.1548 | 0.3745 | -0.6037 | **0.0001** | -0.3124 | 0.0676 | -0.4144 | **0.0133** |
| **Right kidney** | -0.0958 | 0.5843 | -0.5378 | **0.0009** | 0.0913 | 0.6018 | -0.3230 | 0.0584 | 0.0001 | 0.9995 | -0.4340 | **0.0092** |
| **Left kidney** | -0.1172 | 0.5027 | -0.5118 | **0.0017** | 0.1994 | 0.2508 | -0.1868 | 0.2826 | 0.1389 | 0.4262 | -0.3604 | **0.0334** |
| **Liver** | 0.0840 | 0.6313 | 0.0011 | 0.9949 | -0.1370 | 0.4327 | -0.4762 | **0.0038** | -0.1861 | 0.2845 | -0.3844 | **0.0226** |
| **Pancreas** | -0.3067 | 0.0731 | -0.1532 | 0.3795 | -0.2681 | 0.1195 | -0.2143 | 0.2164 | -0.3322 | 0.0512 | -0.2331 | 0.1779 |
| **L2 vertebra** | -0.9310 | **< 0.0001** | -0.8192 | **< 0.0001** | -0.9219 | **< 0.0001** | -0.8228 | **< 0.0001** | -0.9282 | **< 0.0001** | -0.8350 | **< 0.0001** |
| **L1 vertebra** | -0.9283 | **< 0.0001** | -0.8183 | **< 0.0001** | -0.9167 | **< 0.0001** | -0.8229 | **< 0.0001** | -0.9227 | **< 0.0001** | -0.8300 | **< 0.0001** |
| **Left erector spinae** | -0.4448 | **0.0074** | -0.4164 | **0.0128** | -0.4064 | **0.0154** | -0.3428 | **0.0438** | -0.4220 | **0.0116** | -0.3832 | **0.0231** |
| **Right erector spinae** | -0.3709 | **0.0283** | -0.3641 | **0.0315** | -0.3588 | **0.0343** | -0.3541 | **0.0369** | -0.3864 | **0.0219** | -0.3531 | **0.0375** |
| **Left iliopsoas** | -0.3252 | 0.0566 | -0.3308 | 0.0522 | -0.3918 | **0.0199** | -0.3183 | 0.0624 | -0.3157 | 0.0647 | -0.4036 | **0.0162** |
| **Right iliopsoas** | -0.4600 | **0.0054** | -0.0623 | 0.7223 | -0.3280 | 0.0544 | -0.2319 | 0.1800 | -0.4981 | **0.0023** | -0.3850 | **0.0224** |
| **PCN** | 0.0677 | 0.6991 | 0.3552 | **0.0363** | -0.0714 | 0.6835 | 0.2073 | 0.2322 | -0.1124 | 0.5205 | 0.3083 | 0.0716 |

HU: Hounsfield Unit; PCN: pancreatic cystic neoplasm; VNC: virtual non-contrast reconstruction

maximum $HU_{error}$ of ±15 HU. In the venous phase, 33/35 cases were within the range of ±5 HU, and the remaining 2/35 cases had a maximum $HU_{error}$ of ±10 HU. The histograms illustrating the number of patients in each category can be found in Additional file 1 (Supplementary Fig. 23).

### Analysis of the liver

The liver showed higher $HU_{VNC[arterial]}$ compared to $HU_{unenhanced}$, however, the $HU_{error}$ was only 4.64±2.85 HU. For the portal and venous phases, the $HU_{error}$ values were even lower, only 2.12±2.60 HU, and 2.50±2.22 HU, respectively. The $HU_{VNC}$ values showed a very strong correlation with the $HU_{unenhanced}$ in all phases (Table 4). Meanwhile, the $HU_{error}$ had no significant correlation with $HU_{unenhanced}$ in either phase, and it showed only a moderate correlation with $HU_{portal}$ and a weak correlation with $HU_{venous}$ (Table 5).

The $HU_{error}$ values were within a maximum of ±10 HU in all cases in all contrast phases. In the arterial phase, 17/35 cases had a $HU_{error}$ less than ±5 HU, in the portal venous phase, it was 31/35, while the best results were found in the venous phase, where 32/35 cases were within the range of ±5 HU. The histograms illustrating the number of patients in each category can be found in Additional file 1 (Supplementary Fig. 23).

### Intraclass correlation coefficient analysis

The results of ICC analysis showed that most organs had at least one postcontrast phase VNC reconstruction that showed good-to-excellent reproducibility based on the lower value of the 95% confidence interval. Except the vertebrae, spleen, and kidneys which consistently resulted in poor ICC values, and the paraspinal muscles that showed excellent ICC values but with wide confidence intervals. The results of the ICC analysis can be found in Table 6.

In the arterial phase, the ICC analysis showed excellent reliability for the pancreatic parenchyma with an ICC of 0.90 [0.80–0.95]. Good reliability was found for PCNs with ICC of 0.76 [0.43–0.89]) and for iliopsoas muscles with ICCs of 0.79 [0.59–0.89], and 0.75 [0.56–0.87]). However, the remaining organs showed wide confidence intervals. In the portal venous phase, only the liver showed excellent reliability with an ICC of 0.93 [0.70–0.97], other organs either had low ICC values or wide 95% confidence intervals. While in the venous phase, only the liver and pancreas showed good reproducibility with ICC of 0.93 [0.46–0.98], and 0.92 [0.42–0.98], respectively.

Bland-Altman plots further supported the results of the ICC analysis (Supplementary Figs. 19–22 of Additional file 1). All cases were distributed around a $HU_{error}$ close to zero, with almost all measurements within ±1.96 SD; except for vertebrae, kidneys, and spleen, which showed

**Table 6** Interclass correlation coefficient analysis based on the average density values of real unenhanced scans and VNC reconstructions

| | $HU_{VNC[unenhanced]}$ | | $HU_{VNC[arterial]}$ | | $HU_{VNC[portal]}$ | | $HU_{VNC[venous]}$ | |
|---|---|---|---|---|---|---|---|---|
| **Organ** | **ICC** | **95% CI** | **ICC** | **95% CI** | **ICC** | **95% CI** | **ICC** | **95% CI** |
| **Spleen** | 0.31 | [-0.04–0.60] | 0.47 | [0.12–0.71] | 0.21 | [-0.08–0.48] | 0.46 | [0.15–0.69] |
| **Right kidney** | 0.72 | [0.51–0.85] | 0.31 | [-0.09–0.63] | 0.15 | [-0.09–0.43] | 0.10 | [-0.07–0.34] |
| **Left kidney** | 0.69 | [0.47–0.83] | 0.27 | [-0.07–0.56] | 0.18 | [-0.09–0.46] | 0.13 | [-0.08–0.40] |
| **Liver** | 0.83 | [-0.03–0.95] | 0.84 | [-0.01–0.96] | 0.93 | [0.70–0.97] | 0.93 | [0.46–0.98] |
| **Pancreas** | 0.93 | [0.86–0.96] | 0.90 | [0.80–0.95] | 0.82 | [0.30–0.93] | 0.92 | [0.42–0.98] |
| **L2 vertebra** | 0.16 | [-0.03–0.50] | 0.17 | [-0.03–0.51] | 0.17 | [-0.03–0.52] | 0.17 | [-0.03–0.51] |
| **L1 vertebra** | 0.16 | [-0.03–0.49] | 0.17 | [-0.03–0.51] | 0.17 | [-0.03–0.52] | 0.17 | [-0.03–0.51] |
| **Left erector spinae** | 0.87 | [-0.02–0.97] | 0.84 | [-0.04–0.96] | 0.88 | [0.00–0.97] | 0.90 | [0.02–0.97] |
| **Right erector spinae** | 0.86 | [-0.02–0.97] | 0.84 | [-0.04–0.96] | 0.89 | [0.01–0.97] | 0.90 | [0.04–0.98] |
| **Left iliopsoas** | 0.79 | [0.62–0.89] | 0.79 | [0.59–0.89] | 0.76 | [0.21–0.91] | 0.72 | [0.06–0.90] |
| **Right iliopsoas** | 0.81 | [0.65–0.90] | 0.75 | [0.56–0.87] | 0.71 | [0.26–0.87] | 0.64 | [0.04–0.86] |
| **PCN** | 0.91 | [0.82–0.95] | 0.76 | [0.43–0.89] | 0.49 | [-0.04–0.76] | 0.59 | [-0.04–0.84] |

HU: Hounsfield Unit; PCN: pancreatic cystic neoplasm; VNC: virtual non-contrast reconstruction

a huge $HU_{error}$, which was significantly affected by the mean of the measurements.

## Comparison of image quality

### *Subjective evaluation of image quality*

During the subjective assessment of the 35 CT examinations, the expert radiologist found that the VNC reconstructions were smoother and more blurred compared to the real unenhanced scans. The expert radiologist reported the presence of kidney stones in 10 cases, while, 5 had pancreas calcification, 3 had PCNs with mural calcification, and 2 had PCNs with central calcification. The size of the kidney stones was between 1.9 and 6.9 mm, the pancreatic calcifications evaluated had sizes between 1.9 and 3.5 mm, the mural calcifications had sizes between 2.0 and 2.5 mm, while the two central calcifications had sizes of 2.0 and 6.5 mm on the real unenhanced scans. Comparing the measured diameters of these 20 lesions on the real unenhanced scans vs. VNC reconstructions, the unenhanced phase VNC yielded acceptable results with no significant difference (2.98±1.41 mm vs. 2.48±1.19 mm, $p$=0.067), while the arterial, portal, and venous phase VNC reconstructions showed significantly lower measured diameters with 1.64±1.54 mm, 1.65±1.33 mm, and 1.57±1.50 mm each with $p$<0.001, respectively.

The expert radiologist rated the image quality on the basis of the radiological assessability of the calcifications according to a 5-point scale. If more than one calcification or more than one kidney stone was presented, the one with the worst assessability on VNC was reported. Therefore, 20 lesions were evaluated in this subanalysis. As a result, the VNC reconstructed from the real unenhanced scans showed acceptable image quality with an average point of 4.3/5.0. From the postcontrast phase VNC reconstructions, the arterial phase had the highest image quality with an average point of 2.65/5.0, followed by the portal venous phase VNC with 2.45/5.0 points on average, while the venous phase VNC showed the worst image quality with average points of 2.4/5.0. A total number of 7/20 lesions resulted in full subtraction in either of the postcontrast phase VNC reconstructions. Although none of the calcifications were fully subtracted from the VNC reconstructions generated from the unenhanced phase scans, the number of fully subtracted calcifications was 6/20 on the arterial phase VNCs, 4/20 on the portal venous phase VNCs, and 7/20 on the venous phase VNCs.

During the subjective reading of the scans, the radiologist found that the Liver-VNC algorithm was less reliable in patients with chronic pancreatitis. During iodine subtraction the algorithm struggled to differentiate calcifications from the iodine contrast material, lowering the density values of small calcifications and blurring their borders (Fig. 2). In kidneys, special attention should be paid to the density values of stones which may also be reduced on the VNC reconstructions (Fig. 3). From the kidneys that showed marked contrast enhancement, the algorithm failed to subtract the iodine contrast which remained detectable in the renal cortex even on VNC reconstructions (Fig. 4). Meanwhile, the algorithm markedly reduced the densities of those kidneys that showed less pronounced contrast enhancement (Fig. 5). Furthermore, in cases where the spleen had marked striking wave-like contrast enhancement, the Liver-VNC algorithm markedly decreased the density values of the highly enhancing areas (Fig. 6).

### *Quantitative evaluation of image quality*

The subjective impression of smoother images for VNC reconstructions compared to the real unenhanced scans was supported by the results of the quantitative

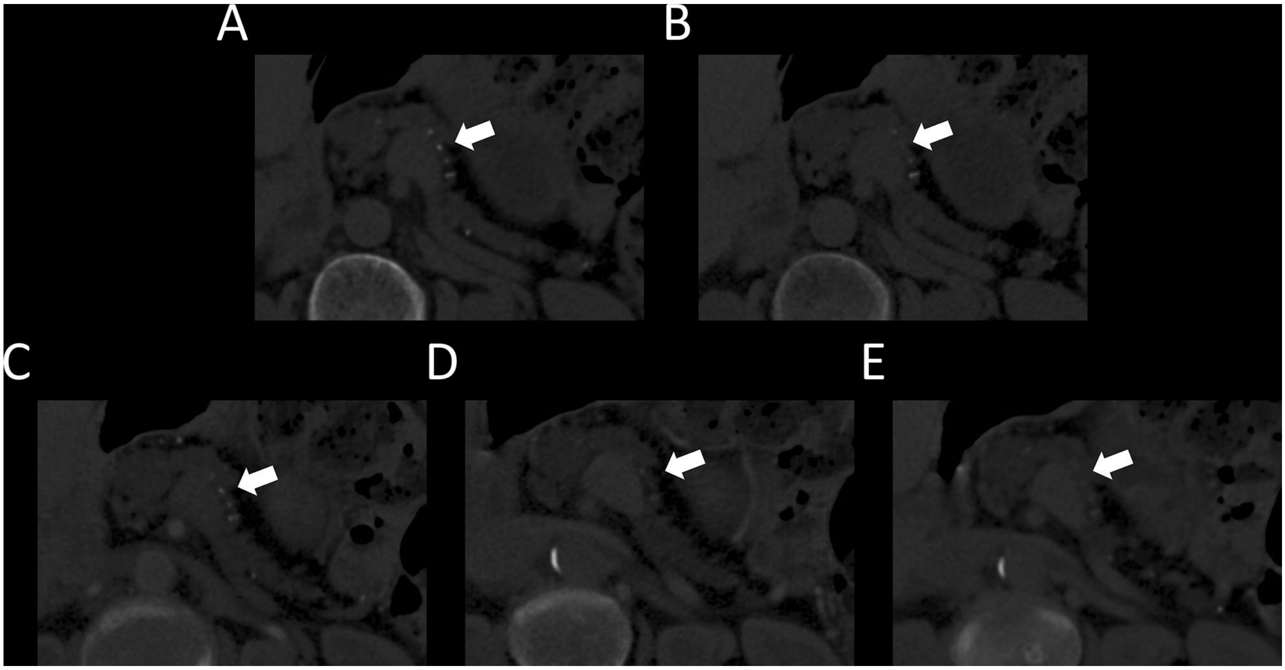


**Fig. 2** Illustration of the limitation of the Liver-VNC algorithm in pancreatic calcifications. Pancreatic calcifications on the unenhanced phase CT scan of a patient with chronic pancreatitis (**A**). The algorithm blurred the margins and decreased the size of the calcifications (arrow) during the reconstruction of the virtual non-contrast images from the unenhanced phase (**B**) arterial phase (**C**), portal phase (**D**), and venous phase (**E**) postcontrast CT scans

assessment of image noise by calculating the CNR. The $CNR_{VNC[unenhanced]}$ was found to be significantly lower compared to the $CNR_{unenhanced}$ values for the kidneys ($p=0.016$), pancreas ($p=0.041$), vertebrae ($p<0.0001$), iliopsoas muscles ($p=0.013$), and PCNs ($p=0.03$). The CNR resulted in significantly lower values on the portal venous phase and venous phase VNC reconstructions compared to the real unenhanced scans for all organs. On the arterial phase, only the vertebrae showed significantly lower $CNR_{VNC[arterial]}$ values (Table 7).

The comparison of the SNR between VNC reconstructions and real unenhanced scans showed heterogeneous results for the different organs on different phases (Table 8). The $SNR_{VNC[unenhanced]}$ were significantly higher for the spleen ($p<0.0001$), kidneys ($p<0.0001$, $p<0.0001$), liver ($p<0.0001$), pancreas ($p<0.0001$), paraspinal muscles ($p<0.0001$), and iliopsoas muscles ($p<0.0001$) compared to the $SNR_{unenhanced}$, while no significant difference was found in the vertebrae and PCNs. For all postcontrast phases, the muscles showed significantly higher $SNR_{VNC}$ values, while the kidneys and PCNs had significantly lower $SNR_{VNC}$ values compared to $SNR_{unenhanced}$.

## Discussion

In our study, we analyzed 12 abdominal organs to investigate whether VNC images reconstructed from arterial, portal, and venous phase spectral CT scans using the Liver-VNC algorithm can replace real unenhanced scans in abdominal imaging., moreover, we directly compared VNC reconstructions of unenhanced phase scans with real unenhanced scans. The difference in density values between the VNC and real unenhanced scans was significant for all postcontrast scans in the kidneys, liver, vertebrae, paraspinal muscles, and PCNs. However, the $HU_{error}$ was only 2.12±2.60 HU and 2.5±2.22 HU for the liver on the portal venous and venous phases, respectively. The density values of the VNC reconstructions also showed a strong to very strong correlation with those on the real unenhanced scans in all investigated organs except the spleen, and kidneys. Finally, we also highlighted the most common pitfalls of VNC reconstructions including the subtraction of kidney stones, pancreatic calcifications, PCN calcifications; and the impaired iodine contrast subtraction from the kidneys and spleen that can limit the introduction of the algorithm to daily clinical practice. Hence, this study contributes to the emerging body of literature evaluating the feasibility and potential of VNC reconstructions of PCD-CT examinations.

By the visual inspection of the reconstructed images, we found that the VNC reconstructions had a more blurred appearance compared to the real unenhanced scans which is supported by the results of the quantitative image noise assessment analysis, as the CNR proved to be significantly lower for all organs in all phases in accordance with the results of existing literature [10, 17].

Previous publications quantitatively validating the reliability of VNC reconstructions mainly focused on the comparison of average HU density values of the

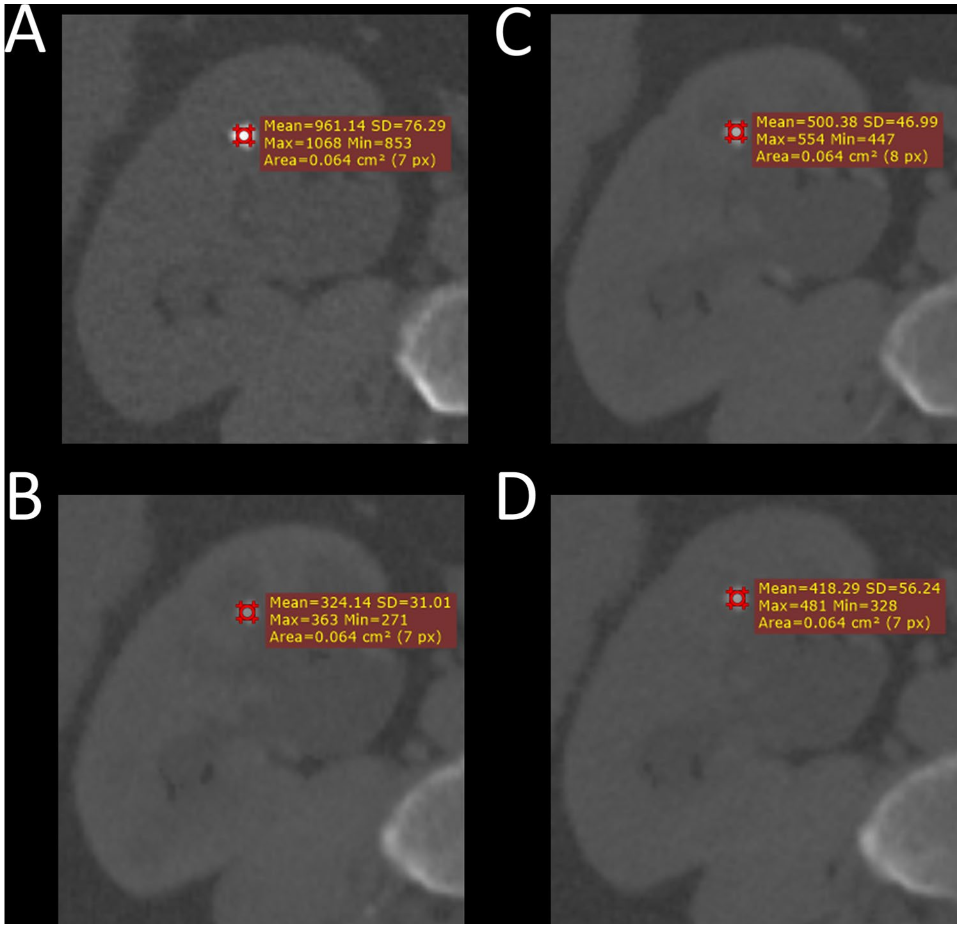


**Fig. 3** Illustration of the limitation of the Liver-VNC algorithm in kidney stones. The difference in the density of a kidney stone between the real unenhanced phase CT series (**A**) and the virtual non-contrast reconstructions generated from the arterial phase (**B**), portal phase (**C**), and venous phase (**D**) series

investigated organs. Niehoff et al. [11] tested the prior version VNC algorithm of the same PCD-CT model. The authors reported significant differences between $HU_{VNC}$ and $HU_{unanhanced}$ in both the arterial and venous phase scans for all the investigated organs. In our study, we confirmed significant differences between $HU_{VNC}$ and $HU_{unanhanced}$ in the spleen in the arterial and portal phases, and in the paraspinal muscles, kidneys, liver, and vertebrae in all three postcontrast phases (Table 3). However, in our study, the $HU_{VNC}$ of paraspinal muscles and the liver showed a markedly stronger correlation with $HU_{unanhanced}$ ($r>0.90$) on all postcontrast phases. These differences can be explained by the fact that we used the Liver-VNC algorithm of the vendor instead of its previous VNC algorithm, therefore our results suggest that this software version may be more reliable.

In their recently published study, Schoenbeck et al. [12] compared the performance of the prior VNC algorithm and the later Liver-VNC algorithm in various abdominal organs. This study was based on the same PCD-CT model of the vendor that we used. The authors found significant differences between $HU_{VNC[unenhanced]}$ and $HU_{unenhanced}$ in the liver, renal cortex, aorta, paraspinal muscle, and subcutaneous fat, but reported no significant differences in the spleen using the VNC algorithm. On the contrary, in our study, by using the Liver-VNC algorithm we found no significant differences in the kidneys, pancreas, iliopsoas muscles, and PCNs, however, we confirmed significant differences in the liver and paraspinal muscles, and we also reported significant differences in the spleen and vertebrae. The authors found significant differences between $HU_{VNC[portal]}$ and $HU_{unenhanced}$, whether the earlier VNC or the later Liver-VNC algorithm was used in all organs except the paraspinal muscles. In our study, we confirmed the significant difference in all organs in the portal venous phase and that the algorithm decreases the density of the kidneys and increases the density of the liver. Moreover, we also investigated the correlation of the $HU_{error}$ with $HU_{unenhanced}$ and $HU_{postcontrast}$ values.

Interestingly, a previous study on a dual-energy CT scanner by Lin et al. [8]. investigating the kidneys obtained contrary results. They found similar cortical

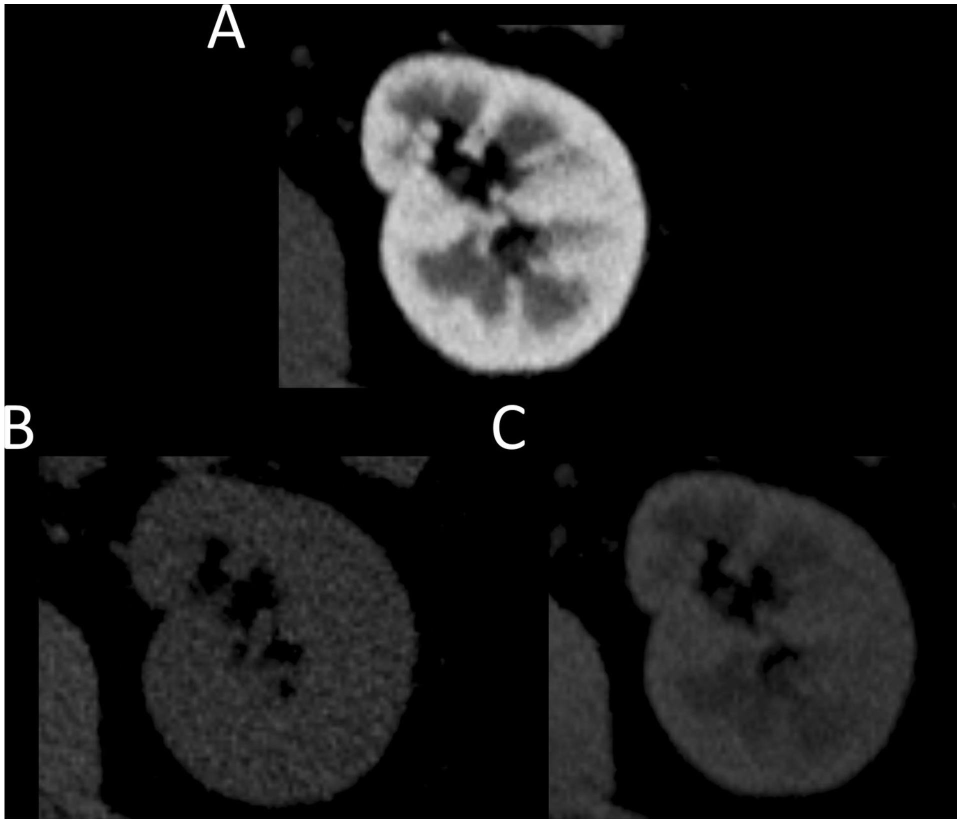


**Fig. 4** Illustration of the failure of the Liver-VNC algorithm for iodine contrast subtraction from kidneys. The left kidney on an arterial phase CT scan (**A**), and the difference between the real unenhanced phase CT scans (**B**) and the virtual non-contrast reconstruction (**C**)

$HU_{VNC}$ values in the corticomedullary phase and significantly increased cortical $HU_{VNC}$ in the nephrographic phase. Although the average $HU_{error}$ values that Lin et al. reported on the corticomedullary phase were only −0.4 HU and 3.1 HU for the cortex and medulla, they had wide ranges of -21.7−22.7 HU and −30.0−21.2 HU. This discrepancy can be at least partially explained by the difference in contrast injection timing and flow rates which affects the $HU_{error}$ values as we demonstrated by correlating the $HU_{error}$ with the $HU_{postcontrast}$ values.

The ranges of $HU_{error}$ in our study were categorized as ±5 HU, ±5–10 HU, ±10–15 HU, ±15–20 HU, and >20 HU. Comparing these results to those published by Çamlıdağ on VNC reconstructions of dual-energy CTs on the nephrographic phase [19], slightly better results were found in our study for the liver and spleen, comparable results for the pancreas, and slightly worse results for the kidneys. The authors reported that 25/142 and 4/142 of the cases had density differences of >10 HU and >20HU for the liver, while in our study, none of the cases had $HU_{error}$ larger than ±10 HU. This difference may be explained with that we used the Liver-VNC algorithm which takes the fat into account during material decomposition. For the spleen, the authors reported that 27/142 and 2/142 cases had density differences of >10 HU and >20 HU, while in our study, all the cases were within the range of ±10HU on the arterial and venous phases, and only 3/35 cases had $HU_{error}$ larger than ±10 HU on the portal venous phase. For the kidneys, approximately half of the cases showed a $HU_{error}$ larger than ±10HU in our study, while Çamlıdağ reported that only 24/142 and 34/142 patients had density difference>10 HU for the left and right kidneys, respectively.

We consider the observed $HU_{error}$ acceptable for the liver, as in daily clinical practice, the CT-based rough assessment of the presence of significant hepatic steatosis relies on the average density measurement on the unenhanced phase scans with a threshold of <40 HU [20]. An average density measurement error of approximately 2–4 HU that we reported may not increase the false positive findings of hepatic steatosis, however, our current research did not aim to cover the detailed reliability analysis of the algorithm in fatty liver disease, therefore, further investigation is needed in this field.

The density measurement of the pancreatic parenchyma on unenhanced CTs can help radiologists diagnose pancreatic lipomatosis. As the $HU_{error}$ was only −1.47±4.87 HU for the arterial phase, -4.9±5.9 HU for the portal phase, and −3.33±2.95 HU for the venous phase VNC reconstructions in our study, we suggest that

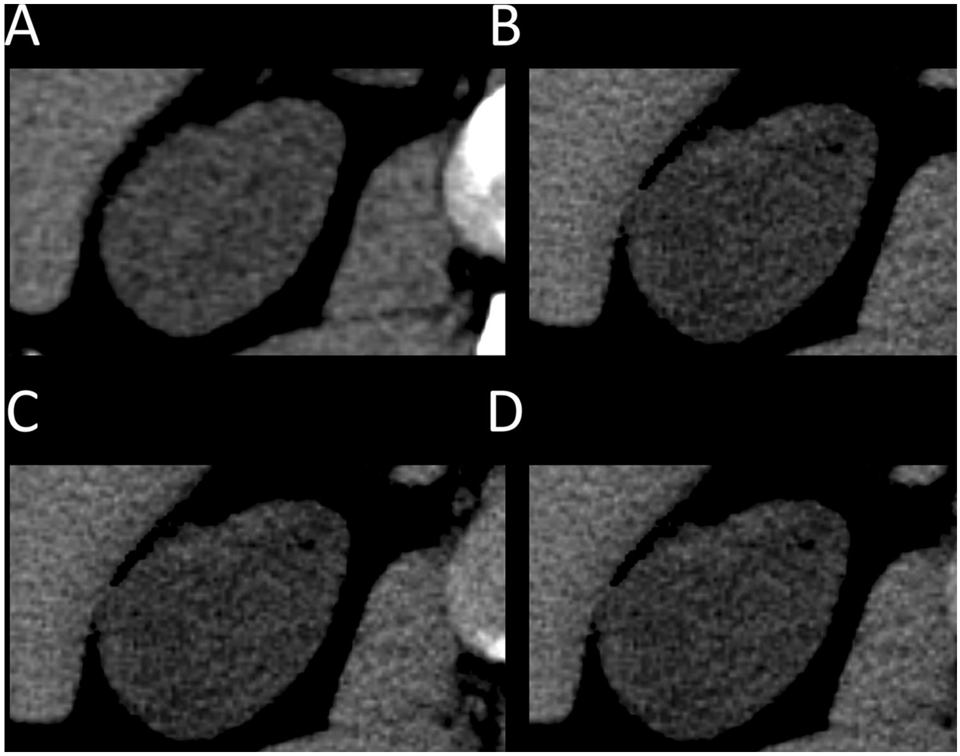


**Fig. 5** Illustration of the excessive decrease in density values during iodine contrast extraction from kidneys by the Liver-VNC algorithm. The difference in the density of the kidney between the real unenhanced phase CT scans (**A**) and the virtual non-contrast reconstructions of arterial phase (**B**), portal phase (**C**), and venous phase (**D**) scans. The algorithm decreased the mean densities

it would not increase the false positive findings of pancreatic lipomatosis. Similarly, the average density measurement of the paraspinal muscles on unenhanced CT has a role in the diagnostics of fatty infiltration of the muscles, however in our study, the Liver-VNC algorithm tended to increase the density values of the paraspinal muscles.

The measurement of lower average density values of the kidney parenchyma on unenhanced CT scans, the so-called "pale kidney sign" is an additional finding that can suggest renal edema and urinary obstruction. Therefore the dramatic decrease of average density values on the VNC reconstructions that we reported may affect the diagnosis. Moreover, the inappropriate contrast-subtraction can cover small renal stones resulting in false negative findings.

The assessment of calcifications on unenhanced phase CT scans is crucial in the diagnostics of pancreatic cystic neoplasms [13], moreover reading the unenhanced phase CT scans is also critical in the diagnostics of chronic calcifying pancreatitis [21], and the characterization of kidney stones [22]. Therefore, our study had a special focus on the semi-quantitative analysis of VNC reconstructions' image quality regarding the radiological evaluation of such small calcifications. The iodine-based contrast media and calcium-containing structures (vertebrae, calcifications) have low differences in spectral attenuation, and the k-edge of iodine and calcium are close to each other [23]. Therefore, the Liver-VNC algorithm cannot differentiate between the two perfectly during material decomposition which is a well-known limitation. For a more detailed description of the k-edge imaging and its limitations, we kindly refer the readers to the recently published methodological paper of Jost et al. [23]. This limitation had the most noticeable effect on the vertebrae in our study which resulted in significantly lower HU values on the VNC reconstructions compared to real unenhanced scans, which can affect the assessment of CT-based osteoporosis. Due to this limitation, the algorithm was less reliable in the assessment of central or mural calcifications of PCNs, and in patients with chronic pancreatitis, where it struggled to differentiate calcified lesions from iodine, lowering the density values of small calcifications, blurring their borders, or even fully subtracting them (Fig. 2) resulting in a clearly inferior image quality during semi-quantitative assessment. This finding complies with those reported by Mileto et al., who assessed the image quality of VNC reconstructions of a dual-energy scanner in pancreas imaging and also reported the partial subtraction of small pancreatic calcifications in 2 cases [24]. We also observed that in the case of high-density calcium stones in the kidney, the Liver-VNC algorithm markedly lowered the density

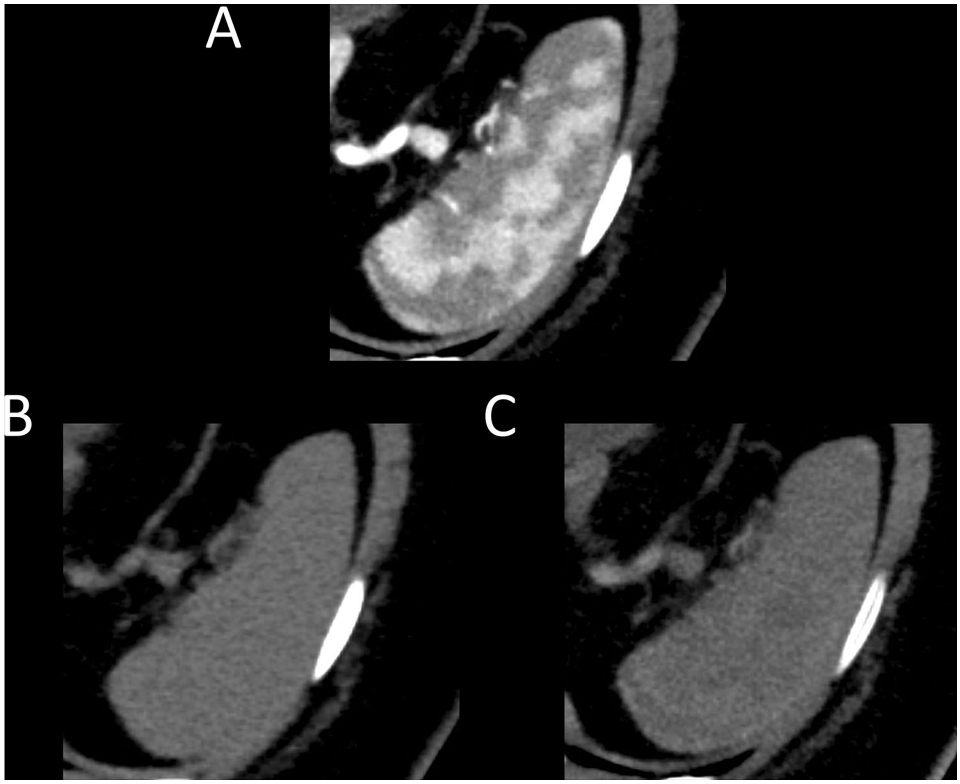


**Fig. 6** Illustration of the failure of the Liver-VNC algorithm for iodine contrast subtraction from the spleen. The striking wave-like contrast enhancement pattern of the spleen on the arterial phase (**A**) scan. The difference in the density of the spleen on the real unenhanced phase CT scans (**B**) and the virtual non-contrast reconstructions generated from the arterial phase (**C**)

**Table 7** Contrast-to-noise ratio of the organs on the virtual non-contrast reconstructions and the real unenhanced CT

| | $HU_{unenhanced}$ | $HU_{VNC[unenhanced]}$ | | $HU_{VNC[arterial]}$ | | $HU_{VNC[portal]}$ | | $HU_{VNC[venous]}$ | |
|---|---|---|---|---|---|---|---|---|---|
| **Organ** | **CNR** | **CNR** | ***p*-value** | **CNR** | ***p*-value** | **CNR** | ***p*-value** | **CNR** | ***p*-value** |
| **Spleen** | 17.70 ± 3.64 | 17.26 ± 3.77 | 0.1412 | 17.05 ± 3.58 | 0.4387 | 12.17 ± 1.78 | **< 0.0001** | 15.70 ± 2.93 | **0.0017** |
| **Right kidney** | 15.82 ± 3.32 | 15.11 ± 3.35 | **0.0155** | 14.53 ± 3.21 | 0.0552 | 10.27 ± 1.64 | **< 0.0001** | 12.74 ± 2.51 | **< 0.0001** |
| **Left kidney** | 15.68 ± 3.25 | 14.94 ± 3.23 | **0.0155** | 14.42 ± 3.18 | 0.0552 | 10.21 ± 1.64 | **< 0.0001** | 12.69 ± 2.48 | **< 0.0001** |
| **Liver** | 18.62 ± 4.02 | 18.44 ± 4.15 | 0.6028 | 18.30 ± 4.28 | 0.4387 | 13.20 ± 2.12 | **< 0.0001** | 16.74 ± 3.26 | **0.0046** |
| **Pancreas** | 15.24 ± 3.21 | 14.64 ± 3.21 | **0.0410** | 14.39 ± 3.57 | 0.1260 | 10.25 ± 1.92 | **< 0.0001** | 13.13 ± 2.81 | **0.0003** |
| **L2 vertebra** | 51.39 ± 14.33 | 30.08 ± 8.02 | **< 0.0001** | 29.99 ± 7.88 | **< 0.0001** | 22.23 ± 4.93 | **< 0.0001** | 27.87 ± 7.23 | **< 0.0001** |
| **L1 vertebra** | 49.79 ± 14.06 | 29.69 ± 7.95 | **< 0.0001** | 29.61 ± 7.74 | **< 0.0001** | 21.97 ± 4.87 | **< 0.0001** | 27.57 ± 7.10 | **< 0.0001** |
| **Left erector spinae** | 16.17 ± 3.43 | 16.08 ± 3.35 | 0.7497 | 16.20 ± 3.97 | 0.5988 | 11.73 ± 1.86 | **< 0.0001** | 14.79 ± 2.88 | **0.0144** |
| **Right erector spinae** | 16.20 ± 3.33 | 16.10 ± 3.28 | 0.7497 | 16.21 ± 3.90 | 0.5988 | 11.72 ± 1.79 | **< 0.0001** | 14.79 ± 2.87 | **0.0138** |
| **Left iliopsoas** | 17.77 ± 3.67 | 16.91 ± 3.64 | **0.0129** | 16.82 ± 3.79 | 0.1260 | 12.22 ± 1.88 | **< 0.0001** | 15.41 ± 2.97 | **0.0003** |
| **Right iliopsoas** | 17.58 ± 3.58 | 16.74 ± 3.53 | **0.0129** | 16.67 ± 3.71 | 0.1260 | 12.09 ± 1.77 | **< 0.0001** | 15.22 ± 2.89 | **0.0003** |
| **PCN** | 14.23 ± 3.31 | 13.59 ± 3.33 | **0.0297** | 13.10 ± 3.35 | 0.0552 | 9.18 ± 1.57 | **< 0.0001** | 11.73 ± 2.52 | **< 0.0001** |

* p-value corrected according to the Benjamini-Hochberg method

The results are reported as mean ± standard deviation

HU: Hounsfield Unit; PCN: pancreatic cystic neoplasm; VNC: virtual non-contrast reconstruction

values of the stones (Fig. 3) which can have therapeutic consequences. This observed phenomenon is in accordance with the findings of Dodig et al. [25] and Gezer et al. [26] who reported accuracies of 72.41–80.46% [25] and a sensitivity of 66.7% [26] for VNC reconstructions in the detection of kidney stones when compared to the real unenhanced scans.

The inaccuracies of the algorithm discussed above can be a major limitation of the application in pancreas imaging and kidney stone assessment. To overcome this limitation, the two main directions are improving the current VNC algorithms designed for iodine-based contrast-enhanced images, and the development of alternative contrast materials. On one hand, the introduction

**Table 8** Signal-to-noise ratio of the organs on the virtual non-contrast reconstructions and the real unenhanced CT

| | $HU_{unenhanced}$ | $HU_{VNC[unenhanced]}$ | | $HU_{VNC[arterial]}$ | | $HU_{VNC[portal]}$ | | $HU_{VNC[venous]}$ | |
|---|---|---|---|---|---|---|---|---|---|
| **Organ** | **SNR** | **SNR** | ***p*-value** | **SNR** | ***p*-value** | **SNR** | ***p*-value** | **SNR** | ***p*-value** |
| **Spleen** | 3.02 ± 0.85 | 3.42 ± 0.94 | **< 0.0001** | 2.95 ± 0.69 | 0.3815 | 2.49 ± 0.61 | **< 0.0001** | 2.99 ± 0.77 | 0.3215 |
| **Right kidney** | 1.93 ± 0.56 | 2.15 ± 0.66 | **< 0.0001** | 1.55 ± 0.47 | **< 0.0001** | 1.16 ± 0.53 | **< 0.0001** | 1.24 ± 0.67 | **< 0.0001** |
| **Left kidney** | 1.78 ± 0.62 | 1.98 ± 0.74 | **< 0.0001** | 1.41 ± 0.47 | **< 0.0001** | 1.06 ± 0.55 | **< 0.0001** | 1.15 ± 0.70 | **< 0.0001** |
| **Liver** | 3.90 ± 0.93 | 4.43 ± 0.97 | **< 0.0001** | 4.09 ± 0.82 | **0.0024** | 3.40 ± 0.65 | **< 0.0001** | 3.87 ± 0.75 | 0.5756 |
| **Pancreas** | 1.29 ± 0.91 | 1.48 ± 0.99 | **< 0.0001** | 1.28 ± 0.87 | 0.6288 | 1.01 ± 0.72 | **< 0.0001** | 1.18 ± 0.87 | **0.0020** |
| **L2 vertebra** | 1.34 ± 0.20 | 1.35 ± 0.20 | 0.4036 | 1.34 ± 0.21 | 0.8537 | 1.34 ± 0.21 | 0.3561 | 1.37 ± 0.22 | **0.0319** |
| **L1 vertebra** | 1.38 ± 0.19 | 1.40 ± 0.20 | 0.0792 | 1.39 ± 0.21 | 0.3815 | 1.38 ± 0.21 | 0.9291 | 1.42 ± 0.22 | **0.0013** |
| **Left erector spinae** | 1.28 ± 0.76 | 1.59 ± 0.89 | **< 0.0001** | 1.57 ± 0.84 | **< 0.0001** | 1.45 ± 0.74 | **< 0.0001** | 1.55 ± 0.81 | **< 0.0001** |
| **Right erector spinae** | 1.28 ± 0.73 | 1.59 ± 0.87 | **< 0.0001** | 1.58 ± 0.81 | **< 0.0001** | 1.45 ± 0.71 | **< 0.0001** | 1.55 ± 0.78 | **< 0.0001** |
| **Left iliopsoas** | 2.68 ± 0.91 | 2.96 ± 1.02 | **< 0.0001** | 2.92 ± 0.9 | **0.0002** | 2.48 ± 0.64 | **0.0047** | 2.81 ± 0.82 | **0.0283** |
| **Right iliopsoas** | 2.19 ± 0.79 | 2.43 ± 0.84 | **< 0.0001** | 2.45 ± 0.65 | **< 0.0001** | 2.13 ± 0.51 | 0.9291 | 2.3 ± 0.63 | **0.0095** |
| **PCN** | 1.08 ± 0.60 | 1.18 ± 0.72 | 0.0792 | 0.85 ± 0.83 | **0.0195** | 0.45 ± 0.79 | **< 0.0001** | 0.53 ± 0.70 | **< 0.0001** |

* p-value corrected according to the Benjamini-Hochberg method

The results are reported as mean ± standard deviation

HU: Hounsfield Unit; PCN: pancreatic cystic neoplasm; VNC: virtual non-contrast reconstruction

of a VNC algorithm specifically designed to preserve calcifications in parenchymal organs and the development of a VNC algorithm optimized for organs showing marked contrast-enhancement (e.g. kidney, spleen) would be important future research directions. On the other hand, the usage of iodine-based contrast materials is a severe limitation of spectral imaging-based material decomposition due to their suboptimal spectral attenuation range. Therefore, the field of developing new, alternative contrast materials also gained increasing attention in the literature [23]. A phantom study by Amato et al. [27] demonstrated that contrast agents with higher atomic numbers such as gadolinium could serve as a better alternative for PCD-CT. Moreover, Kim et al. [28] also proved that the reconstructed contrast maps successfully differentiated gadolinium from iodine and calcium. These phantom studies demonstrate that the introduction of new imaging protocols using alternative contrast agents could successfully overcome the limitations of calcium subtraction in the reconstruction of VNC images and contrast agent maps in the future.

Our study has some limitations that must be taken into consideration. Our study had a retrospective study design with a low number of cases including a special population of patients with PCNs. The evaluation of the reliability of VNC reconstructions in special pathologies of the given abdominal organs e.g. different stages of liver fibrosis in the case of the liver, degree of sarcopenia in the case of the muscles, or chronic renal failure in the case of the kidneys were out of the scope of our current research. In our study, the small number of patients did not allow us to investigate the effect of contrast agent concentration and contrast agent injection flow rate on the reliability of the Liver-VNC algorithm. Our study was based on the three-dimensional volumetric assessment of organs focusing on the changes in average HU density values caused by the Liver-VNC algorithm that affect the entire organ. This method, however, cannot capture fine differences between real unenhanced scans and VNC reconstructions such as the subtraction of small-size calcifications and kidney stones. The limitation of the Liver-VNC algorithm in these cases was observed by an expert radiologist during the subjective reading of real unenhanced scans and VNC reconstructions. The number of patients with these lesions in our study did not allow statistical analysis, but the limitations of VNC reconstructions in these cases are important and may prevent the widespread clinical use of VNC. Therefore, further studies based on larger patient populations are needed in this field.

## Conclusions

In conclusion, our study confirmed the results of previous literature in the case of the liver parenchyma analysis, as we demonstrated the reliability of mean density measurement on VNC reconstruction especially in the portal and venous phases. The results of our study also demonstrated that the degree of enhancement on postcontrast scans as well as the base enhancement on the unenhanced scans affect the reliability of VNC reconstructions for several organs. Although mean density measurements on VNC reconstructions were found to be reliable in at least one postcontrast phase for most organs, further improvements are needed before the VNC reconstructions can be introduced to clinical applications in abdominal imaging and can be utilized to examine the spleen, kidneys, and vertebrae.

### Abbreviations

CNR Contrast-to-Noise Ratio
EID-CT Energy Integrating Detector CT

| | |
|---|---|
| HU | Hounsfield Unit |
| ICC | Intraclass Correlation Coefficient |
| PCD-CT | Photon-Counting Detector CT |
| PCN | Pancreas Cystic Neoplasm |
| ROI | Region of Interest |
| SD | Standard Deviation |
| SNR | Signal-to-Noise Ratio |
| VNC | Virtual Non-Contrast |

## Supplementary Information

The online version contains supplementary material available at https://doi.org/10.1186/s12880-024-01419-w.

Supplementary Material 1

Supplementary Material 2

**Acknowledgements**
Not applicable.

**Author contributions**
I.D. – Conceptualization, Investigation, Methodology, Roles/Writing - original draft; L.S. – Data curation, Project administration, Roles/Writing - original draft; M.B. – Data curation, Roles/Writing - original draft; Á.Sz. – Investigation, Writing - review & editing; P.N.K. – Methodology, Writing - review & editing; A.S. – Resources, Writing - review & editing; P.M.H. – Funding acquisition, Resources, Writing - review & editing; B.K.B. – Conceptualization, Methodology, Formal analysis, Visualization, Project administration, Supervision, Roles/Writing - original draft; All authors approved the final version of the manuscript.

**Funding**
This research did not receive any specific grant from funding agencies in the public, commercial, or not-for-profit sectors.

**Data availability**
Data is provided within the manuscript or supplementary information files.

## Declarations

**Ethics approval and consent to participate**
The Ethics Committee of our University (Semmelweis University Regional and Institutional Committee of Science and Research Ethics) has approved the present study (RKEB: 256./2023). The need for informed consent was waived by the Ethics Committee (Semmelweis University Regional and Institutional Committee of Science and Research Ethics).

**Consent for publication**
Not applicable.

**Competing interests**
The authors declare no competing interests.

Received: 10 February 2024 / Accepted: 2 September 2024
Published online: 09 September 2024

**References**

1. Leng S, Bruesewitz M, Tao S, Rajendran K, Halaweish AF, Campeau NG, et al. Photon-counting detector CT: System Design and clinical applications of an Emerging Technology. Radiographics: Rev Publication Radiological Soc North Am Inc. 2019;39(3):729–43.
2. Flohr T, Petersilka M, Henning A, Ulzheimer S, Ferda J, Schmidt B. Photon-counting CT review. Physica Medica: PM : an international journal devoted to the applications of physics to medicine and biology. Official J Italian Association Biomedical Phys (AIFB). 2020;79:126–36.
3. van der Bie J, van Straten M, Booij R, Bos D, Dijkshoorn ML, Hirsch A, et al. Photon-counting CT: review of initial clinical results. Eur J Radiol. 2023;163:110829.
4. Boyce CJ, Pickhardt PJ, Kim DH, Taylor AJ, Winter TC, Bruce RJ, et al. Hepatic steatosis (fatty liver disease) in asymptomatic adults identified by unenhanced low-dose CT. AJR Am J Roentgenol. 2010;194(3):623–8.
5. Tirkes T, Shah ZK, Takahashi N, Grajo JR, Chang ST, Venkatesh SK, et al. Reporting standards for Chronic Pancreatitis by using CT, MRI, and MR Cholangiopancreatography: the Consortium for the study of chronic pancreatitis, diabetes, and pancreatic Cancer. Radiology. 2019;290(1):207–15.
6. Ouzaid I, Al-qahtani S, Dominique S, Hupertan V, Fernandez P, Hermieu JF, et al. A 970 Hounsfield units (HU) threshold of kidney stone density on non-contrast computed tomography (NCCT) improves patients' selection for extracorporeal shockwave lithotripsy (ESWL): evidence from a prospective study. BJU Int. 2012;110:E438–42. (11 Pt B).
7. De Cecco CN, Muscogiuri G, Schoepf UJ, Caruso D, Wichmann JL, Cannaò PM, et al. Virtual unenhanced imaging of the liver with third-generation dual-source dual-energy CT and advanced modeled iterative reconstruction. Eur J Radiol. 2016;85(7):1257–64.
8. Lin Y-M, Chiou Y-Y, Wu M-H, Huang S-S, Shen S-H. Attenuation values of renal parenchyma in virtual noncontrast images acquired from multiphase renal dual-energy CT: comparison with standard noncontrast CT. Eur J Radiol. 2018;101:103–10.
9. Virarkar MK, Vulasala SSR, Gupta AV, Gopireddy D, Kumar S, Hernandez M, et al. Virtual non-contrast imaging in the Abdomen and the Pelvis: an overview. Seminars in Ultrasound. CT MRI. 2022;43(4):293–310.
10. Mergen V, Racine D, Jungblut L, Sartoretti T, Bickel S, Monnin P, et al. Virtual noncontrast abdominal imaging with photon-counting detector CT. Radiology. 2022;305(1):107–15.
11. Niehoff JH, Woeltjen MM, Laukamp KR, Borggrefe J, Kroeger JR. Virtual non-contrast versus true non-contrast computed tomography: initial experiences with a photon counting scanner approved for clinical use. Diagnostics (Basel Switzerland). 2021;11(12).
12. Schoenbeck D, Pauline Haag N, Elias Michael A, Michael Woeltjen M, Boriesosdick J, Saeed S, et al. Dedicated virtual non-contrast images adapted for liver tissue in clinical photon counting CT improve virtual non-contrast imaging in various organs beyond the liver. Eur J Radiol. 2023;167:111031.
13. European Study Group on Cystic Tumours of the Pancreas. European evidence-based guidelines on pancreatic cystic neoplasms. Gut. 2018;67(5):789–804.
14. Fedorov A, Beichel R, Kalpathy-Cramer J, Finet J, Fillion-Robin JC, Pujol S, et al. 3D slicer as an image computing platform for the quantitative Imaging Network. Magn Reson Imaging. 2012;30(9):1323–41.
15. Wasserthal J, Breit H-C, Meyer MT, Pradella M, Hinck D, Sauter AW et al. TotalSegmentator: Robust Segmentation of 104 Anatomic Structures in CT Images. Radiol: Artif Intell. 2023;5(5):e230024.
16. Holz JA, Alkadhi H, Laukamp KR, Lennartz S, Heneweer C, Püsken M, et al. Quantitative accuracy of virtual non-contrast images derived from spectral detector computed tomography: an abdominal phantom study. Sci Rep. 2020;10(1):21575.
17. Al-Difaie Z, Scheepers MH, Bouvy ND, Engelen S, Havekes B, Postma AA. Can virtual non-contrast imaging replace true non-contrast imaging in multiphase scanning of the neck region? Acta Radiol open. 2023;12(8):20584601231205159.
18. Si-Mohamed S, Dupuis N, Tatard-Leitman V, Rotzinger D, Boccalini S, Dion M, et al. Virtual versus true non-contrast dual-energy CT imaging for the diagnosis of aortic intramural hematoma. Eur Radiol. 2019;29(12):6762–71.
19. Çamlıdağ İ. Compatibility of true and virtual unenhanced attenuation in rapid kV-switching dual energy CT. Diagnostic and interventional radiology (Ankara. Turkey). 2020;26(2):95–100.
20. Hamer OW, Aguirre DA, Casola G, Lavine JE, Woenckhaus M, Sirlin CB. Fatty liver: imaging patterns and pitfalls. Radiographics: Rev Publication Radiological Soc North Am Inc. 2006;26(6):1637–53.
21. Löhr JM, Dominguez-Munoz E, Rosendahl J, Besselink M, Mayerle J, Lerch MM, et al. United European Gastroenterology evidence-based guidelines for the diagnosis and therapy of chronic pancreatitis (HaPanEU). United Eur Gastroenterol J. 2017;5(2):153–99.
22. Tzelves L, Türk C, Skolarikos A. European Association of Urology Urolithiasis Guidelines: where are we going? European urology focus. 2021;7(1):34–8.
23. Jost G, McDermott M, Gutjahr R, Nowak T, Schmidt B, Pietsch H. New contrast media for K-Edge imaging with photon-counting detector CT. Invest Radiol. 2023;58(7):515–22.
24. Mileto A, Mazziotti S, Gaeta M, Bottari A, Zimbaro F, Giardina C, et al. Pancreatic dual-source dual-energy CT: is it time to discard unenhanced imaging? Clin Radiol. 2012;67(4):334–9.

25. Dodig D, Solocki Matić T, Žuža I, Pavlović I, Miletić D, Markić D. Side-by-side evaluation of virtual non-contrast and post-contrast images improves detection of clinically significant urolithiasis on single-phase split bolus dual-energy CT urography. Br J Radiol. 2021;94(1121):20210013.
26. Gezer M, Karaca L, Özdemir Z, Kahraman A, Oğuz F, Erbay MF, et al. Use of dual energy CT urography in evaluation of urinary stone and complex cyst. Turk J Med Sci. 2023;53(1):264–72.
27. Amato C, Klein L, Wehrse E, Rotkopf LT, Sawall S, Maier J, et al. Potential of contrast agents based on high-Z elements for contrast-enhanced photon-counting computed tomography. Med Phys. 2020;47(12):6179–90.
28. Kim J, Bar-Ness D, Si-Mohamed S, Coulon P, Blevis I, Douek P, et al. Assessment of candidate elements for development of spectral photon-counting CT specific contrast agents. Sci Rep. 2018;8(1):12119.

## Publisher's note

Springer Nature remains neutral with regard to jurisdictional claims in published maps and institutional affiliations.